ChemComm

Nanoscale coordination polymers with ligand-centred pH-responses and spin transition

Journal:	*ChemComm*
Manuscript ID:	CC-COM-07-2014-005299
Article Type:	Communication
Date Submitted by the Author:	09-Jul-2014
Complete List of Authors:	Ruiz-Molina, Daniel; CEntro de Investigación en Nanociencia y Nanotecnologia, Novio, Fernando; Institut Català de Nanociència i Nanotecnologia (ICN2-CSIC), Nador, Fabiana; Institut Català de Nanociència i Nanotecnologia (ICN2-CSIC),

Journal Name

RSCPublishing

COMMUNICATION

Nanoscale coordination polymers with ligand-centred pH-responses and spin transition

Cite this: DOI: 10.1039/xoxxoooooox

F. Nador,[a] F. Novio[a,b] and D. Ruiz-Molina*[a,b]

Received ooth January 2012,
Accepted ooth January 2012

DOI: 10.1039/xoxxoooooox

www.rsc.org/

A bis-catechol ligand connected through an imine bond is used to fabricate switchable coordination polymer particles with pH-tuned spin transition responses.

Coordination polymer particles (CPPs) have recently emerged as a novel family of functional nanoparticles.[1] Multifunctionality and chemical flexibility are characteristics of this unique class of highly tailorable functional materials. As such, since first being reported less than a decade ago,[2] amorphous CPPs have already shown their efficacy as encapsulation carriers,[3] building blocks for molecular electronics,[4] precursors for inorganic particles,[5] and theranostics platforms,[6] among many others. Nonetheless, the synthetic methodology for CPPs is in its fledgling stage. One of the most actives areas researchers are actively endeavouring is to develop smart responsive CPPs whose structure and properties can be fined tuned by means of external stimuli, namely pH. So far, various pH-sensitive CPPs that dissolve or collapse in response to pH,[7] have been reported. Though successful, most of the examples reported to date are mainly based on the instability of certain metal-ligand bonds under acidic conditions, which limits the range of materials that can be used. Here we show how using the appropriate multitopic organic ligand makes it possible to structure well-known functional building blocks in the form of spherical particles with pH-responses while retaining the metal-ligand bond.

Valence tautomeric coordination polymer particles were chosen as the test case scenario for these studies. These particles interconvert reversibly upon temperature variations between two electronic isomers in a switchable manner by a reversible intramolecular transfer between the metal ion and the redox-active ligand.[8] Since each electronic isomer has a different magnetic moment[9] and a critical dependence on the local molecular environment (e.g. packing),[10] these complexes are excellent candidates to monitor any variation along the possible particle dissociation process. To achieve this objective we have designed and synthesized a new bis-catechol $\mathbf{L_1}$ (Figure 1a). The interest for this ligand is twofold. First, bis-catechol ligands have already been shown to successfully induce valence tautomerism[11] (VT) and second, fast pH-sensitive cleavage of the imine bond at pH 5-7 while being relatively high stable at pH~8 has already been described for organic polymeric particles.[12] Finally, VT particles with the non pH sensitive ligand $\mathbf{L_2}$ have also been synthesized for comparison purposes.

Ligand $\mathbf{L_1}$ was synthesized by a condensation reaction between dopamine hydrochloride and 3,4-dihydroxybenzaldehyde as shown in Figure 1b (for more details see Supplementary Material S1). Afterwards, its pH-response was tested by placing the ligand in two different solutions at pH~5 (citrate buffer, CBS) and pH~7 (phosphate buffer, PBS). ^{1}H NMR spectra at pH~5 revealed that the signal of the imino proton (8.0 ppm) decreases with time while the intensity of the aldehydic proton (9.6 ppm) increases up to a maximum at 60 min, in agreement with the dissociation of $\mathbf{L_1}$ into its original precursors.

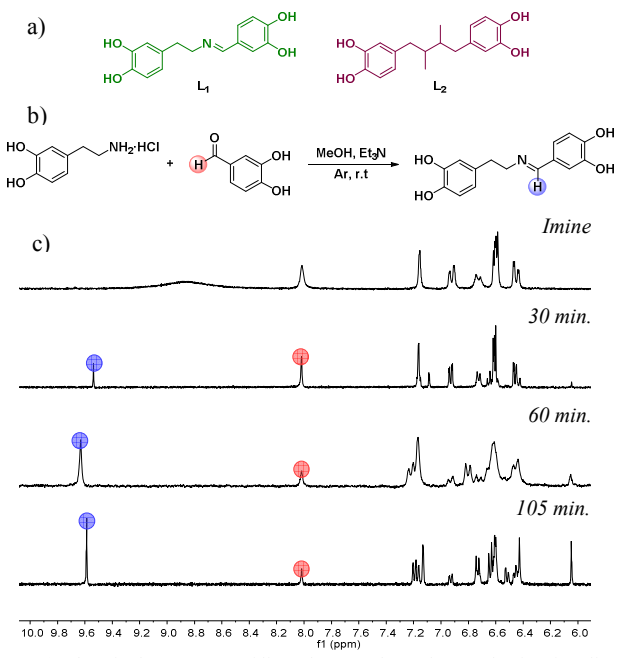

Fig. 1 (a) Chemical structures of ligands $\mathbf{L_1}$ and $\mathbf{L_2}$. (b) Synthesis of $\mathbf{L_1}$ ligand by condensation reaction between dopamine hydrochloride and 3,4-dihydroxybenzaldehyde. (c) Time-dependence ^{1}H NMR of $\mathbf{L_1}$ at pH~5 at the times thereby indicated.

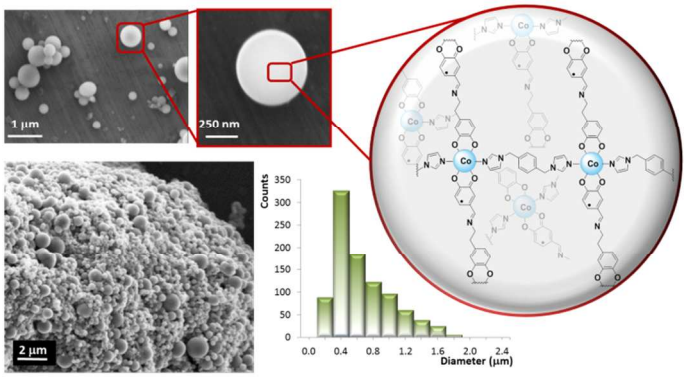

Fig. 2 a) Schematic illustration describing the coordination between ligands bearing several anchor groups (L_1 and bix) and Co(II) to form nanoscale CPPs. b) SEM image and size distribution histogram of **CPP_1**.

Longer exposition times show the formation of additional side-products, most likely tetrahydroisoquinoline (THIQ), associated to the presence of additional Pictet-Spengler cyclization reaction (see Supplementary Material Fig. S1 and S2).[13] On the contrary, exposition of **L_1** to pH~7 indicates that it is stable with less than 20% of the initial aldehydic species recovered after 5 hours (see Fig. S3).

CPPs were fabricated afterwards by interfacial polymerization by mixing an aqueous solution of cobalt acetate with an organic solution (EtOH/DMSO) of 1,4-bis(imidazole-1-ylmethyl)benzene (bix) and **L_1**. The precipitate formed after 3 days was collected, washed several times with water and EtOH, and dried under vacuum resulting in particles (**CPP_1**) with average diameters between 0.2–1.6 µm, as shown by scanning electron microscopy (SEM) (see Fig. 2b). Smaller nanoparticles (average diameter size around 40 nm) can also be obtained by using magnetic stirring technique (see Supplementary Material S3B and Fig. S4). Infrared analysis revealed the introduction of ligand **L_1** within the structure of the new nanoparticles with the presence of bands in the 1275-1289 cm^{-1} range attributed to the C-O stretching of the catecholate mode (see Supplementary Material Fig. S5). Moreover, the lack of bands in the 3460-3240 cm^{-1} region assigned to the O-H stretching as well as the band at 1357 cm^{-1} associated to the O-H bending, confirmed the coordination state of **L_1**. The presence of bix was also verified by the appearance of the typical bands around 3136, 1232 and 1105 cm^{-1} resultant of stretching and bending mode of C-H present in the imidazole and aromatic rings, respectively. Moreover, UV-Vis spectroscopy of **CPP_1** showed clearly the presence of **L_1** ligand through the absorption band centred in 392nm (see Fig S6). X-ray Photoelectron Spectroscopy (XPS) and Energy Dispersive X-ray (EDX) confirmed finally the presence of the cobalt ion (see Supplementary Material Fig. S7 and S8). Worth to mention, elemental analysis on different nanoparticle batches slightly differs from the expected values for a 1:1:1 (L_1:bix:cobalt) ratio (see Fig. 2a and Supplementary Material S3A), fact that has been tentatively attributed to the encapsulation of free ligand molecules or solvent molecules within the particles along its formation process, as already reported.[14]

The pH-response of **CPP_1** was studied in two different buffer solutions at pH~5 (CBS) and pH~7 (PBS) under magnetic stirring. After fixed periods of time the resulting samples were centrifuged and washed several times with water and EtOH. The SEM images of the dispersions at pH~5 at 3 hours already show a remarkable loss of their spherical shape while inducing agglomeration (see Figure 3b). On the contrary, the same particles retain their characteristic spherical shape upon exposition at pH~7 even for 14hs (see Supplementary Material Fig. S9). pH-induced morphological modifications were associated to the disruption of the imine bond, as confirmed by chemical means. Infrared analysis of **CPP_1** did not show any difference before and after exposition at pH~7 for 14 hours whereas significant changes were observed at pH~5 (see Fig. S10 and S11). As expected, the characteristic band at 1645 cm^{-1} of the υC=N of imine as well as the bands at 1486 cm^{-1} (υC=C) and 1099 cm^{-1} (δC-H, bix) disappear with the time. Interestingly, the imine rupture does not affect the coordination bonds as confirmed by magnetization measurements.

Variable-temperature magnetic characterization of **CPP_1** was done on the 15-370 K temperature range operating at a magnetic field strength of 0.1 T (Figure 3a, black squares). At high temperatures, the χT value of 2.07 emu·K·mol^{-1} is close to the expected value for the high-spin [$Co^{II}(DBSQ)_2$]. On cooling, we observe a decrease of χT down to a value of 1.79 emu·K·mol^{-1} at 300 K that is associated with the interconversion from the high-spin [Co^{II}(Semiquinone)] to the low-spin [Co^{III}(Catecholate)] isomer.

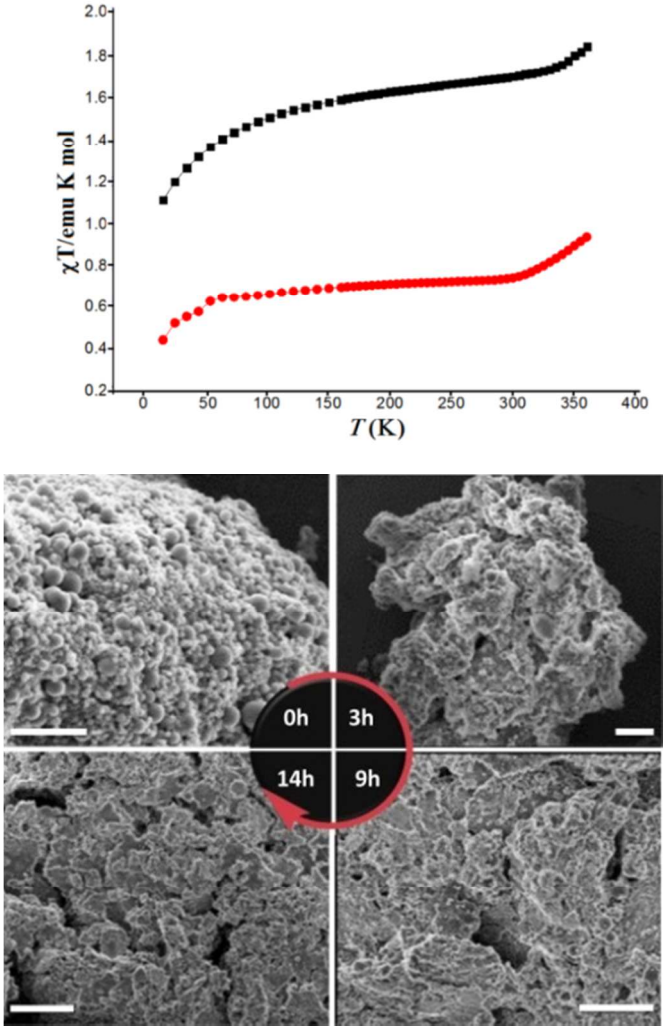

Fig. 3 (Top) χT values as a function of temperature for the pH sensitive **CPP1** before (■) and after acidic treatment for 14h (●). (Bottom) SEM images of **CPP_1** before and after decomposition at pH~5 (CBS buffer) at the times thereby indicated. Scale bars are 4 µm.

Below 200 K, the interconversion continues with smaller diminutions according with the χT value that monotonically decreases down to a value of 1.20 emu·K·mol^{-1} at 15 K. This step-like interconversion is characteristic of amorphous valence tautomeric CPPs. Though, when the same magnetic measurements are done on the pH sensitive nanoparticles after exposure at pH~5 for 14h, the characteristic VT behaviour of most VT samples obtained upon solvent evaporation is found.[10b] As can be seen in Figure 3a, the resulting sample exhibits a χT value essentially independent of temperature and close to the value of 0.5 emu.K.mol^{-1}. Such value confirms that this sample remains mostly on the low-spin [Co^{III}(Catecholate)] form along the whole temperature range. A gradual increase of the χT value takes place at temperatures higher than 300 K, due to the incomplete interconversion to the high-spin [Co^{II}(Semiquinone)] form. Considering that the coordination sphere around the cobalt ion remains unaltered, the different VT behaviour between the amorphous **CPP$_1$** and the product resulting upon imine dissociation can be associated to the matrix modification upon dissociation process.

Finally, to fully confirm that dissociation of **CPP$_1$** takes place because the presence of the pH-sensitive imine bond, novel nanoparticles were fabricated using a related commercial ligand **L$_2$** (norhydroguaiaretic acid), where the imino group is replaced by an alkyl group (see Fig. 1a). Initially, the stability of **L$_2$** under acid condition (pH~5) was tested by ^{1}H NMR, proving to be stable for long time (see Supplementary Material Fig. S12). Afterwards, amorphous nanoparticles (**CPP$_2$**) were also obtained by interfacial polymerization and fully characterized by SEM, FT-IR, EDX and XPS (see Supplementary Material S6). As expected, the pH-response of **CPP$_2$** colloidal suspensions did not reflect any remarkable difference after 24 hours at pH~7 (PBS) none at pH~5 (CBS) under magnetic stirring, as monitored by SEM, FT-IR, UV-Vis and magnetization measurements (see Suplementary Material S7).

Conclusions

pH-sensitive amorphous **CPP** particles with ligand centered responses have been reported for the first time. For this, a flexible bis-catecholate bridging ligand that: I) can induced polymerization, II) assures strong coordination capabilities at different pHs and III) its redox properties allow to monitor the particle dissociation with time, is used. pH-triggered response of the CPP particles resulting from this ligand is therefore ensured by introducing a sensitive imine bridge; in this way, **CPP$_1$** particles turn out to dissociate after a few hours at pH~5 while remain stable at pH~7 for many more hours. Moreover, similar CPP particles without the pH sensitive ligand do not exhibit any response to pH. These results open the door for the use of CPPs with improved performances in well-developed fields such as sensing, drug delivery or molecular electronics, among many others.

Acknowledgments

This work was supported by project MAT2012-38318-C03-02 from the Spanish Government and FEDER funds. F. N. thanks the Ministerio de Ciencia e Innovación (MICINN) for a postdoctoral JdC fellowship. Authors also thank ECOSTBio Cost Action

Notes and references

[a] *ICN2 - Institut Catala de Nanociencia i Nanotecnologia, Campus UAB, 08193 Bellaterra (Barcelona), Spain*

[b] *CSIC - Consejo Superior de Investigaciones Cientificas, ICN2 Building , Campus UAB ,08193 Bellaterra (Barcelona), Spain.*

Electronic Supplementary Information (ESI) available: [Synthetic and experimental procedures, SEM and TEM images, magnetization graphic and NMR, FT-IR, UV-Vis, XPS and EDX spectra]. See DOI: 10.1039/c000000x/

[1] (*a*) M. Y. Masoomi and A. Morsali, *RSC Adv.*, 2013, **3**, 19191; (*b*) W. Lin, W. J. Rieter and K. M. L. Taylor, *Angew. Chem. Int. Ed.*, 2009, **48**, 650; (*c*) A. M. Spokoyny, D. Kim, A. Sumrein and C. A. Mirkin, *Chem. Soc. Rev.*, 2009, **38**, 1218.

[2] (*a*) M. Oh and C. A. Mirkin, *Nature*, 2005, **438**, 651; (*b*) X. Sun, S. Dong and E.Wang, *J. Am. Chem. Soc.*, 2005, **127**, 13102.

[3] (*a*) I. Imaz, J. Hernando, D. Ruiz-Molina and D. Maspoch, *Angew. Chem., Int. Ed.*, 2009, **48**, 2325; (*b*) C. Jo, H. J. Lee and M. Oh, *Adv. Mater.*, 2011, **23**, 1716; (*c*) R. Nishiyabu, C. Aimé, R. Gondo, T. Noguchi and N. Kimizuka, *Angew. Chem., Int. Ed.*, 2009, **48**, 9465.

[4] (*a*) F. Prins, M. Monrabal-Capilla, E. A. Osorio, E. Coronado and H. S. J. van der Zant, *Adv. Mater.*, 2011, **23**, 1545; (*b*) I. Boldog, A. Gaspar, V. Martínez, P. Pardo-Ibañez, V. Ksenofontov, A. Bhattacharjee, P. Gütlich and J. A. Real, *Angew. Chem., Int. Ed.*, 2008, **47**, 6433; (*c*) I. A. Gural'skiy, C. M. Quintero, G. Molnár, I. O. Fritsky, L. Salmon and A. Bousseksou, *Chem. Eur. J.*, 2012, **18**, 9946.

[5] (*a*) M. Hu, A. A. Belik, M. Imura, K. Mibu, Y. Tsujimoto and Y. Yamauchi, *Chem. Mater.*, 2012, **24**, 2698; (*b*) W. Cho, Y. H. Lee and M. Oh, *Adv. Mat.* 2011, **23**, 1720; (*c*) J.–U. Park, H. J. Lee, W. Cho, C. Jo and M. Oh, *Adv. Mater.* 2011, **23**, 3161; (*d*) X. Liu, *Angew. Chem., Int. Ed.*, 2009, **48**, 3018.

[6] (*a*) F. Novio, J. Simmchen, N. Vázquez, L. Amorín and D. Ruiz-Molina, *Coord. Chem. Rev.*, 2013, **257**, 2839; (*b*) J. Della Rocca, D. Liu and W. Lin, *Acc. Chem. Res.*, 2011, **44**, 957; (*c*) J. Della Rocca and W. Lin, *Eur. J. Inorg. Chem.*, 2010, 3725.

[7] (*a*) L. Xing, H. Zheng, Y. Cao and S. Che, *Adv. Mater.*, 2012, **24**, 6433; (*b*) P. Fei Gao, L. Ling Zheng, L. Jiao Liang, X. Xi Yang, Y. Fang Li and C. Zhi Huang, *J. Mater. Chem. B*, 2013, **1**, 3202; (*c*) H. Zheng, L. Xing, Y. Cao and S. Che, *Coord. Chem. Rev.*, 2013, **257**, 1933.

[8] I. Imaz, D. Maspoch, C. Rodríguez-Blanco, J. M. Pérez-Falcón, J. Campo and D. Ruiz-Molina, *Angew. Chem., Int. Ed.*, 2008, **47**, 1857.

[9] (*a*) E. Evangelio and D. Ruiz-Molina, *Eur. J. Inorg. Chem.*, 2005, 2957; (*b*) P. Gütlich and A. Dei, *Angew. Chem. Int. Ed. Engl.*, 1997, **36**, 2734.

[10] (*a*) E. Evangelio and D. Ruiz-Molina, *C. R. Chimie*, 2008, **11**, 1137; (*b*) E. Evangelio, C. Rodriguez-Blanco, Y. Coppel, D. N. Hendrickson, J. P. Sutter, J. Campo and D. Ruiz-Molina, *Solid State Sciences*, 2009, **11**,793.

[11] G. Poneti, M. Mannini, B. Cortigiani, L. Poggini, L. Sorace, E. Otero, P. Sainctavit, R. Sessoli and A. Dei, *Inorg. Chem.*, 2013, **52**, 11798.

[12] W. M. Sharman, J. E. van Lier and C. M. Allen, *Adv. Drug. Deliv. Rev.*, 2004, **56**, 53.

[13] (*a*) J. Stöckigt, A. P. Antonchick, F. Wu and H. Waldmann, *Angew. Chem., Int. Ed.*, 2011, **50**, 8538; (*b*) E. D. Cox and J. M. Cook, *Chem. Rev.*, 1995, **95**, 1797.

[14] (*a*) Q. Zhao, H. Li, X. Wang and Z. Chen, *Chem. Lett.*, 2002, **31**, 988; (*b*) L. Amorín-Ferré, F. Busqué, J. L. Bourdelande, D. Ruiz-Molina, J. Hernando and F. Novio, *Chem. Eur. J.*, 2013, **19**, 17508.

Supporting Information for

Coordination polymer particles with ligand-centred pH-responses and spin transition

F. Nador,[a] F. Novio[a,b] and D. Ruiz-Molina*[a,b]

Index

S1. Synthesis of *N*-(3,4-dihydroxybenzylidene)-2-(3,4-dihydroxyphenyl)ethaneamine (L_1)

A mixture of dopamine hydrochloride (1.5 mmol, 284 mg) and 3,4-dihydroxybenzaldehyde (1.5 mmol, 207 mg) in methanol absolute (36 mL) was stirred at room temperature under argon atmosphere. After complete dissolution, triethylamine (1.5 mmol, 210 μL) was slowly added by syringe. After six hours a yellow solid started to precipitate. The reaction was left overnight under magnetic stirring and after that the methanol was evaporated under reduced pressure. The solid was washed with water (3x10 mL), filtered and dried to obtain L_1: 83% yield. ^{1}H NMR: δ = 2.68 (t, *J* = 6.9 Hz, 2H), 3.63 (t, *J* = 6.9 Hz, 2H), 6.45 (d, *J* = 7.7 Hz, 1H), 6.60-6.61 (m, 2H), 6.73 (d, *J* = 8.0 Hz, 1H), 6.93 (d, *J* = 8.0 Hz, 1H), 7.17 (s, 1H), 8.01 (s, 1H). ^{13}C NMR: δ = 35.8, 53.2, 109.0, 112.5, 117.2, 119.8, 121.7, 128.7, 135.5, 144.1, 144.6, 148.4, 164.0, 170.8. IR-KBr (cm^{-1}) 3310.9, 3246.5, 1659.0, 1610.7, 1514.1, 1356.3, 1282.2, 1127.7. Anal. (%) Calcd. for $C_{15}H_{15}NO_4$: C, 65.96; H, 5.49; N, 5.13. Found: C, 65.87; H, 5.37; N, 5.15.

S2. pH-response of L_1 monitored by ^{1}H NMR

Nuclear magnetic resonance (NMR) spectra were recorded on a Bruker ARX-400 and ARX-250 spectrophotometer using methanol-d_4 and dimethyl sulfoxide-d_6 as solvent.

S2.1. By-product obtained after exposure L_1 at pH~5 treatment

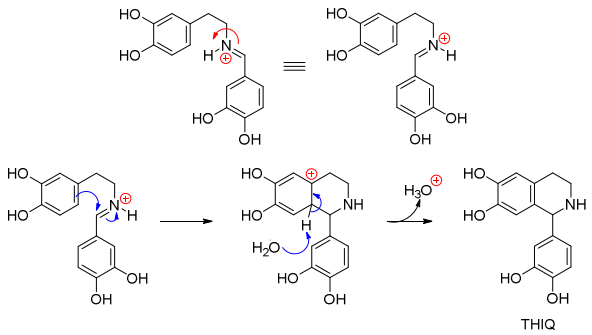

Figure S1. Mechanism of Pictet-Spengler cyclization of **L_1** in acid medium

S2.2. Time dependence stability of L_1 at pH~5

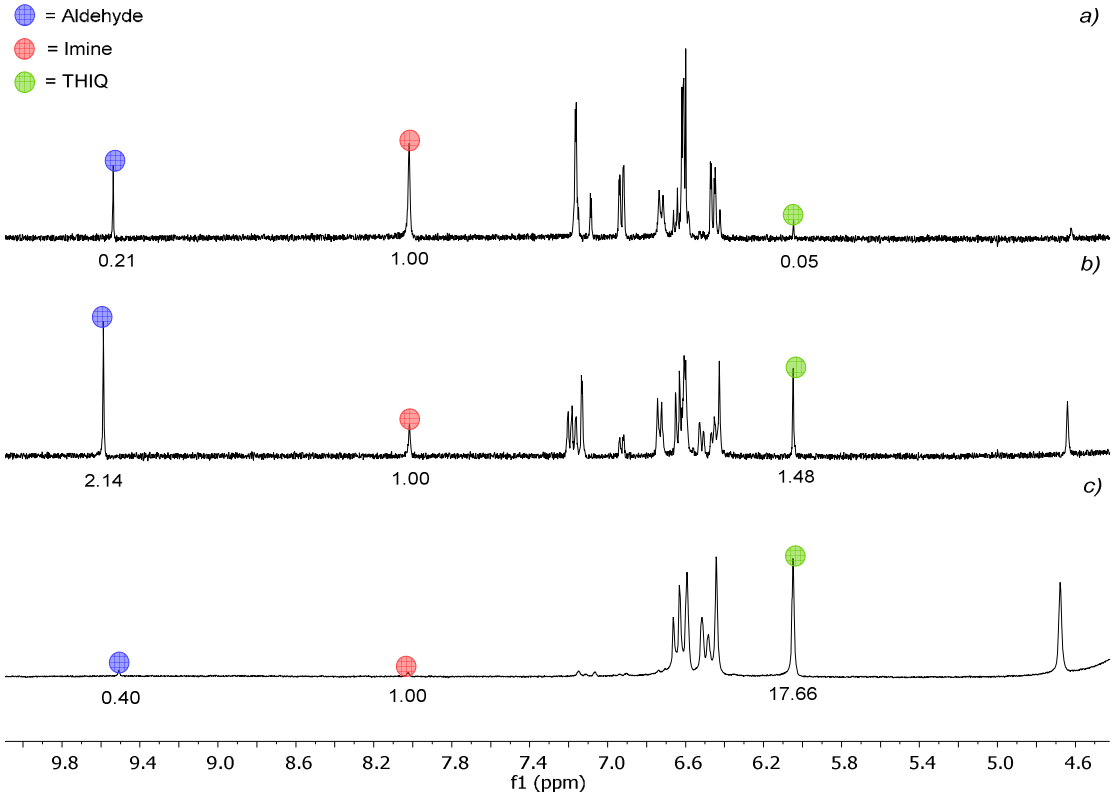

Figure S2. ^{1}H RMN spectra of $\mathbf{L_1}$ at pH~5 after a) 30min, b) 90min and c) 150min. The integrals are shown below the signals.

S2.3. Time dependence stability of L_1 at pH~5 and pH~7

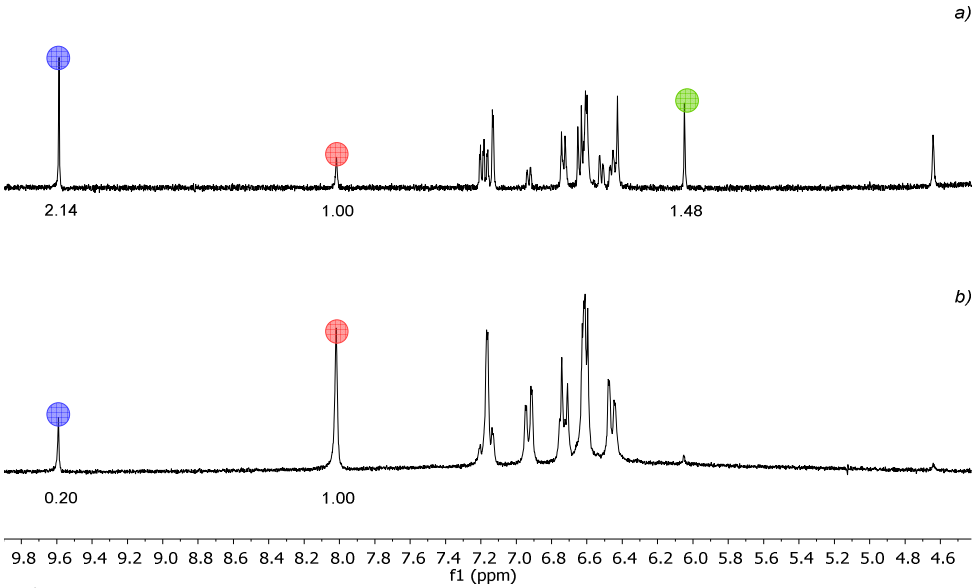

Figure S3. ^{1}H RMN spectra of $\mathbf{L_1}$ after a) 105 min at pH~5 and b) 300 min at pH~7. The integrals are shown below the signals.

3. Synthesis and full characterization of CPP_1

S3.1. Interfacial Polymerization

Synthesis of [Co(Bix)(L_1)] CPP_1: A mixture of **L_1** (0.5 mmol, 136.5 mg) and 1,4-bis(imidazole-1-ylmethyl)benzene (bix, 0.5 mmol, 118.5 mg) was dissolved in DMSO (5 mL), and later ethanol (40 mL) was added. On the other hand, $Co(CH_3COO)_2 \cdot 4H_2O$ (0.5 mmol, 124.6 mg) was placed in a vial of and dissolved in water (5 mL). The mixture of ligands was slowly added on the aqueous solution forming a new phase. A black solid started to form in the interphase, precipitating after few hours. The reaction left during 72h without moving and finally the precipitate was centrifuged (8000 rpm) and washed with water and ethanol several times. The solvent was removed and the solid dried under vacuum. Anal. (%) Calcd. For $C_{29}H_{25}N_5O_4Co$: C, 61.52; H, 4.42; N, 12.36. Found: C, 52.69; H, 3.46; N, 10.59.

S3.2. Magnetic Stirring

Synthesis of [Co(Bix)(L_1)] CPP_1´: A mixture of **L_1** (0.5 mmol, 136.5 mg) and bix (0.5 mmol, 118.5 mg) was dissolved in DMSO (5 mL), and later ethanol (40 mL) was added. Under magnetic stirring (700 rpm) the addition of an aqueous solution of $Co(CH_3COO)_2 \cdot 4H_2O$ (0.5 mmol, 124.6 mg in 5 mL of water) led to a color change to black. Rapidly a fine precipitate was formed and after stirring at room temperature for 24 hours, the precipitate was centrifuged (10000 rpm) and washed with water and ethanol several times. The solvent was removed and the solid dried under vacuum. TEM images of the resulting spherical nanoparticles showed a size distribution around 40 ± 20 nm.

S3.3. SEM (Scanning Electron Microscopy) and TEM (Transmission Electron Miscroscopy)

SEM images were performed on a scanning electron microscope (FEI Quanta 650 FEG) at acceleration voltages of 2–5 kV. Aluminium was used as support.
TEM images were obtained with a FEI Tecnai G2 F20. One drop of a solution of the materials was deposited on a carbon coated copper grid and left to dry. The observation was performed at room temperature at a voltage of 200 kV.

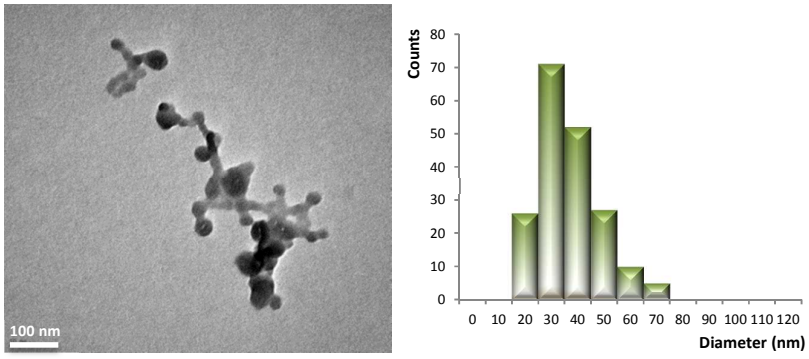

Figure S4. TEM image of **CPP_1´** and histogram with the size distribution

S3.4. FT-IR (Infrared Spectroscopy)

FT-IR spectra were collected on a Tensor 27 FT-IR Spectrometer (Bruker) in the range of 400-4000 cm^{-1} using KBr pellets.

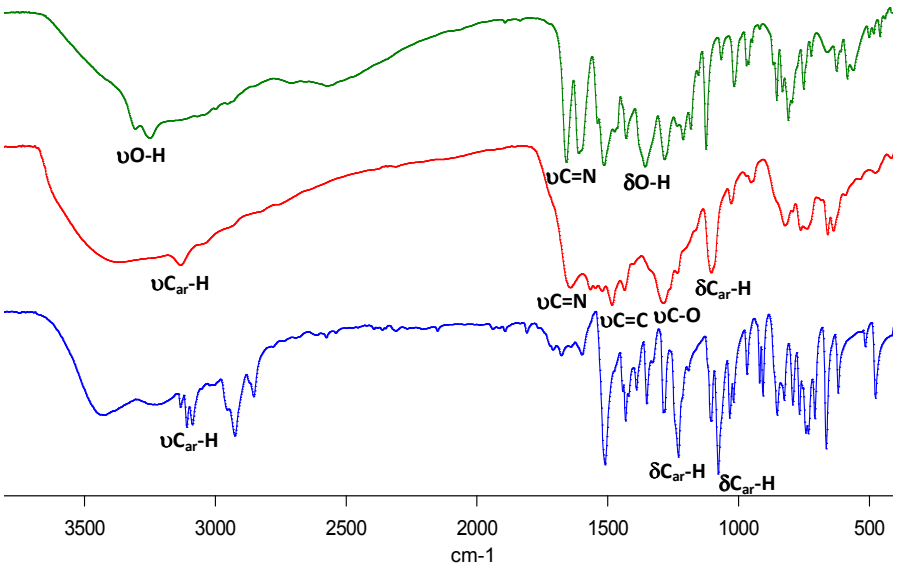

Figure S5. FT-IR of **L$_1$** (—), **CPP$_1$** (—) and bix (—)

*S3.5. UV-Vis (**Ultraviolet–Visible** Spectroscopy)*

UV-Vis spectra were obtained on a Cary 4000 spectrophotometer (Agilent) using quartz cuvettes.

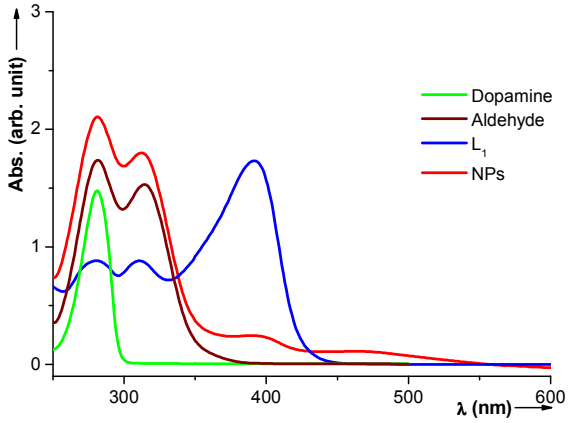

Figure S6. UV-Vis of **CPP$_1$**

S3.6. X-ray Photoelectron Spectroscopy (XPS)

XPS measurements were performed with a Phoibos 150 analyzer (SPECS GmbH, Berlin, Germany) in ultra-high vacuum conditions (base pressure 1E-10mbar) with a monochromatic aluminium Kalpha X-ray source (1486.74eV).

The presence of cobalt was determined by X-ray Photoelectron Spectroscopy (XPS). Firstly, a sample of $Co(CH_3COO)_2 \cdot 4H_2O$ was analysed as reference, and then the **CPP$_1$** and **CPP$_2$**. All the spectra were referenced to the aliphatic carbon at binding energy (BE) of 284.8 eV. High-resolution Co 2p spectrum showed two important signals, the more intense from Co $2p_{3/2}$ at 781.1 eV and the less intense from Co2p1/2 at 796.7 eV. Moreover, two satellite peaks at 785.9 and 802.4 eV were found, which supports even more the presence of Co(II).

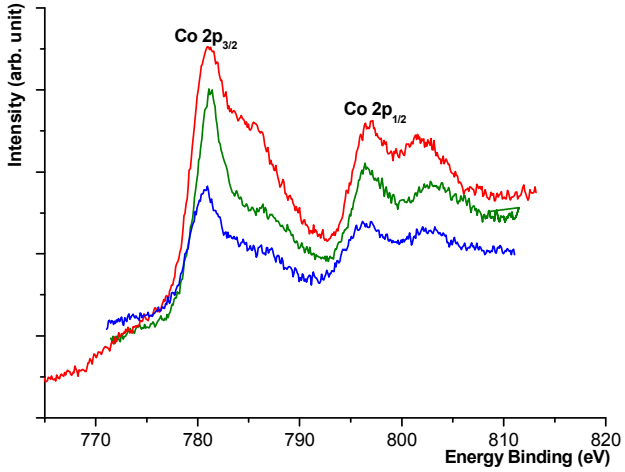

Figure S7. XPS of **CPP_1** (—), **CPP_2** (—) and $Co(AcO)_2 \cdot 4H_2O$ (—)

S3.7 Energy Dispersive X-ray (EDX)

The analysis on several sections confirmed the presence of cobalt, with energy bands of 6.9, 7.7 keV (K lines) and 0.8 keV (L line). The analysis also showed carbon, oxygen and nitrogen.

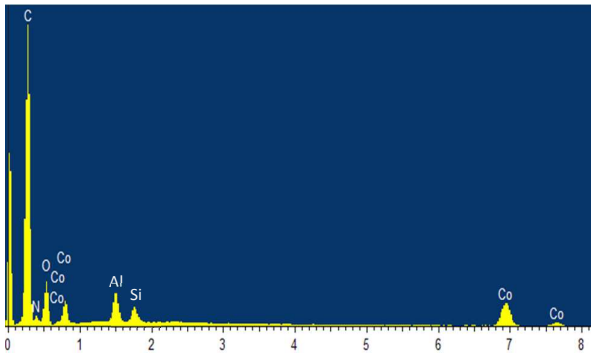

Figure S8. EDX of **CPP_1**. Al and Si peaks come from the Aluminium tape used

S4. pH-response studies of CPP_1

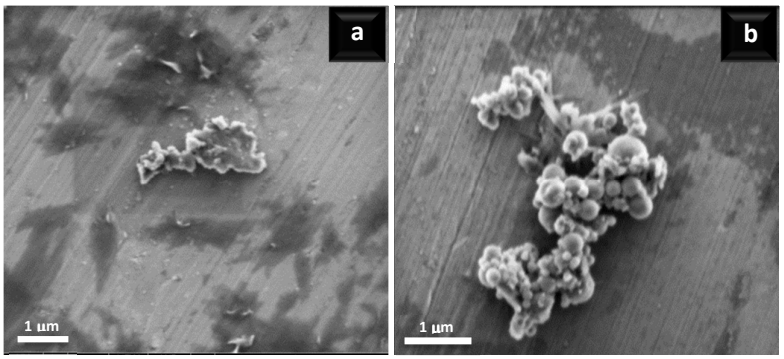

Figure S9. Time dependence stability of **CPP_1** monitored by SEM. (a) after 6h at pH~5 (CBS buffer) and (b) after 14h at pH~7 (PBS buffer)

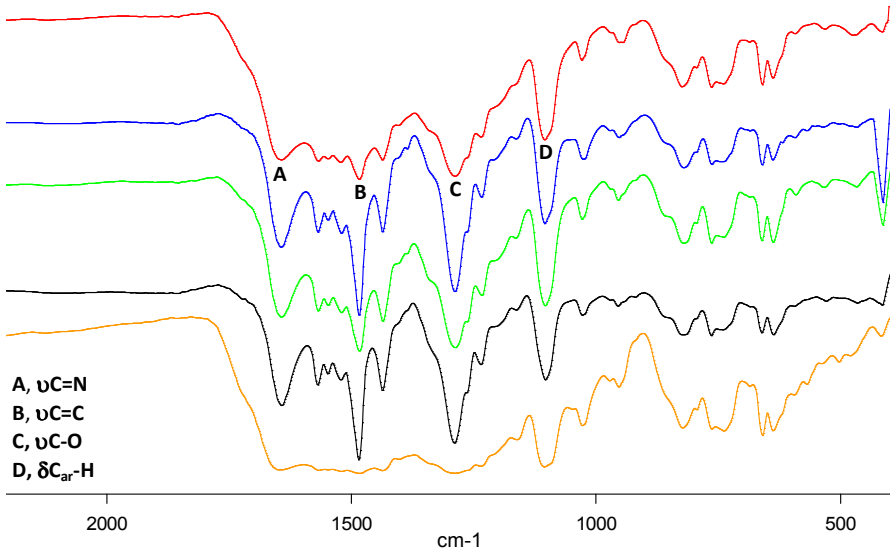

Figure S10. FT-IR of **CPP$_1$** before (—) and after treatment at pH~7 for 3h (—), 6h (—), 9h (—) and 14h (—)

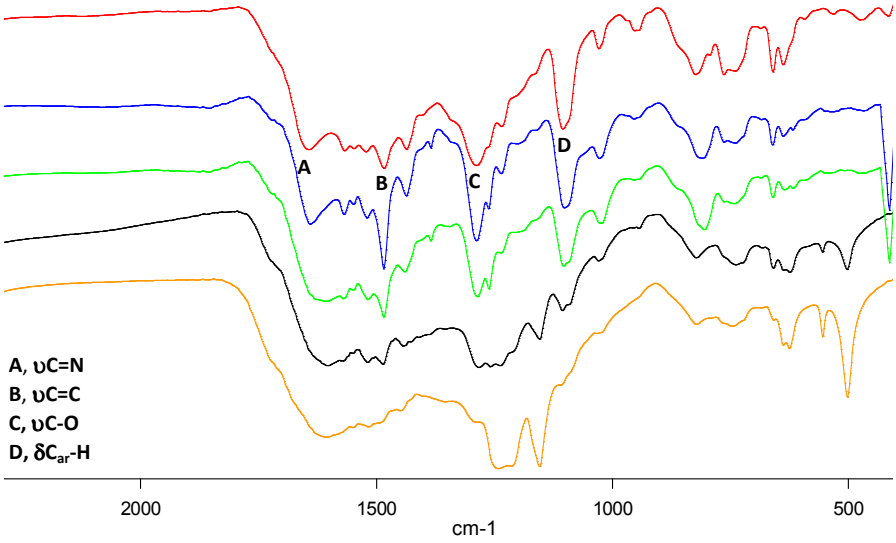

Figure S11. FT-IR of **CPP$_1$** before (—) and after treatment at pH~5 for 3h (—), 6h (—), 9h (—) and 14h (—)

S5. pH-response of L_2 monitored by ^1H NMR

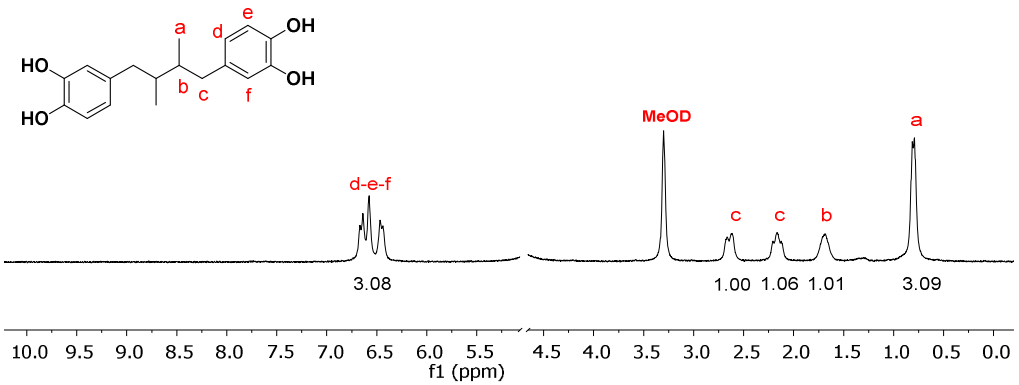

Figure S12. ^1H RMN spectra of **L_2** at pH~5 after 24h. The integrals are shown below the signals

S6. Synthesis and full characterization of CPP_2

S6.1. Interfacial Polymerization

Synthesis of [Co(Bix)(L_2)] CPP_2: A mixture of nordihydroguaiaretic acid (L_2) (0.5 mmol, 151.2 mg) and bix (0.5 mmol, 118.5 mg) was dissolved in ethanol (16 mL). On the other hand, $Co(CH_3COO)_2{\cdot}4H_2O$ (0.5 mmol, 124.6 mg) was placed in a vial and dissolved in water (5 mL). The mixture of ligands was slowly added on the aqueous solution forming a new phase. A grey precipitate started to form in the interphase, precipitating after few hours. The reaction left during 72h without moving and finally the precipitate was centrifuged (8000 rpm) and washed with water and ethanol several times. The solvent was removed and the solid dried under vacuum. Anal. (%) Calcd. For $C_{32}H_{32}N_4O_4Co$: C, 64.54; H, 5.37; N, 9.41. Found: C, 60.03; H, 4.47; N, 8.11.

S6.2. Magnetic Stirring

Synthesis of [Co(Bix)(L_2)] CPP_2': A mixture of **L_2** (0.5 mmol, 151.2 mg) and bix (0.5 mmol, 118.5 mg) was dissolved in ethanol (16 mL). Under magnetic stirring (700 rpm) the addition of an aqueous solution of $Co(CH_3COO)_2{\cdot}4H_2O$ (0.5 mmol, 124.6 mg in 5 mL of water) led to a color change to violet. Rapidly a precipitate was formed and after stirring at room temperature for 24 hours, the precipitate was centrifuged (10000 rpm) and washed with water and ethanol several times. The solvent was removed and the solid dried under vacuum. TEM images of the resulting spherical nanoparticles showed a size distribution around 100 ± 60 nm.

S6.3. SEM and TEM

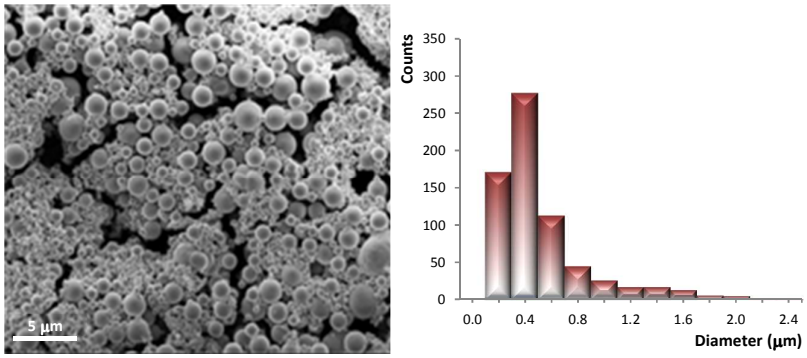

Figure S13. SEM image of **CPP$_2$** and histogram with the size distribution

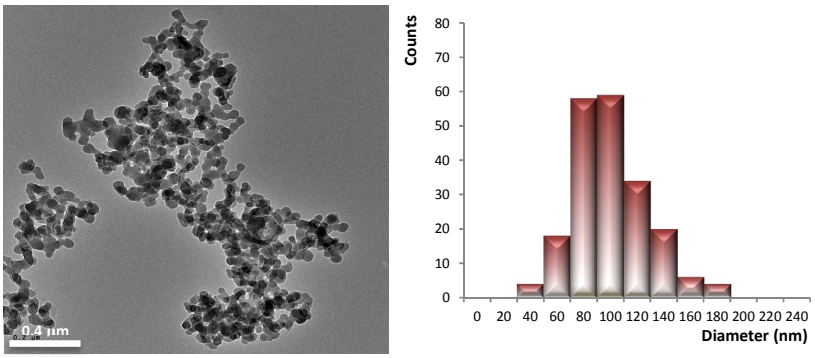

Figure S14. TEM image of **CPP$_2$´** and histogram with the size distribution

S6.4. FT-IR

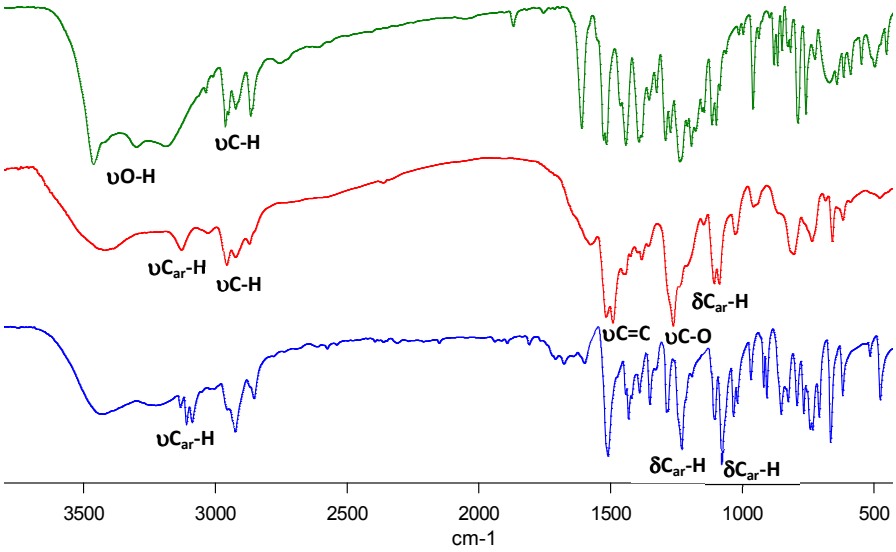

Figure S15. FT-IR of **L$_2$** (—), **CPP$_2$** (—) and bix (—)

S6.5. UV-Vis

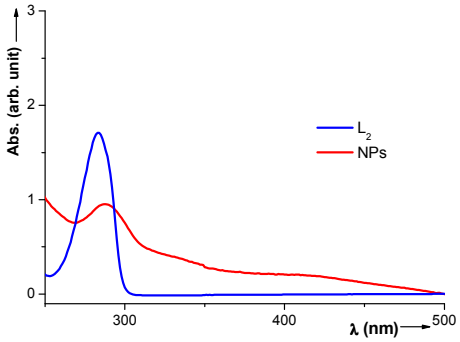

Figure S16. UV-Vis of **CPP_2**

S6.6 EDX

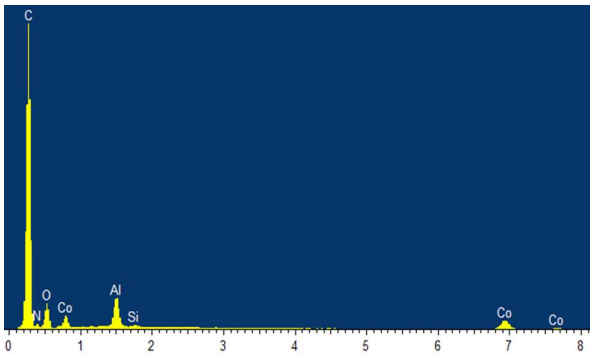

Figure S17. EDX of **CPP_2**. Al and Si peaks come from the Aluminium tape used

7. pH-response studies of CPP_2

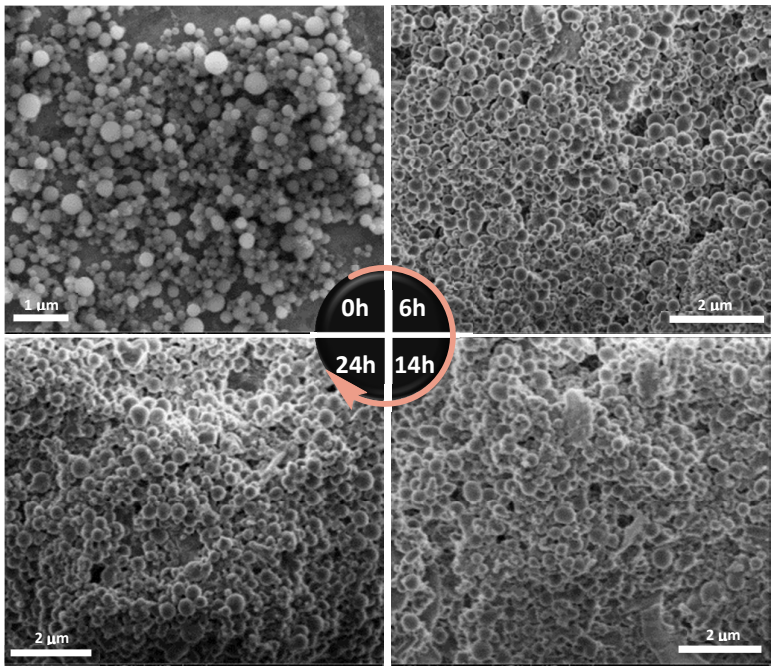

Figure S18. Time dependence stability of **CPP_2** before and after exposure at pH~5 (CBS buffer) at the times thereby indicated

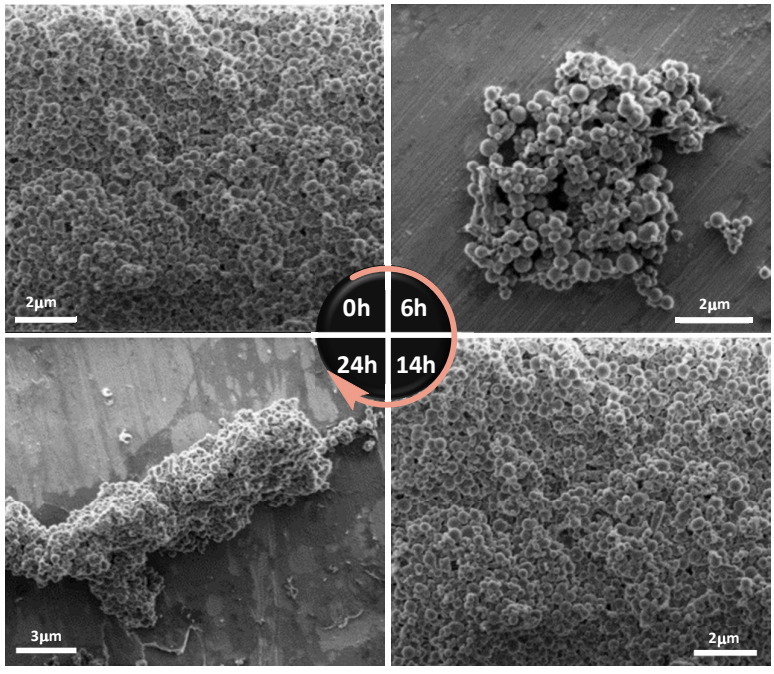

Figure S19. Time dependence stability of **CPP_2** before and after exposure at pH~4 (MES buffer) at the times thereby indicated

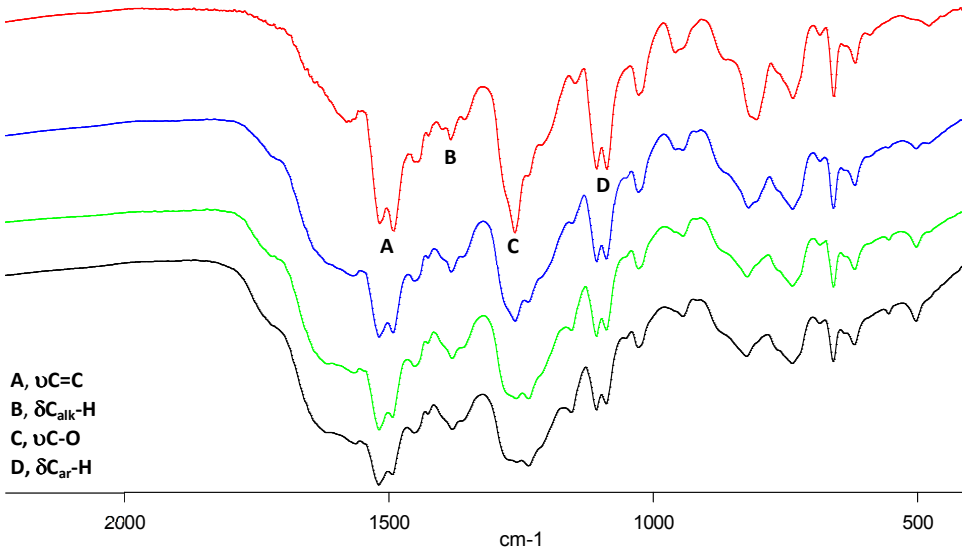

Figure S20. FT-IR of **CPP$_2$** before (—) and after treatment at pH~5 for 4.3h (—), 9h (—) and 24h (—)

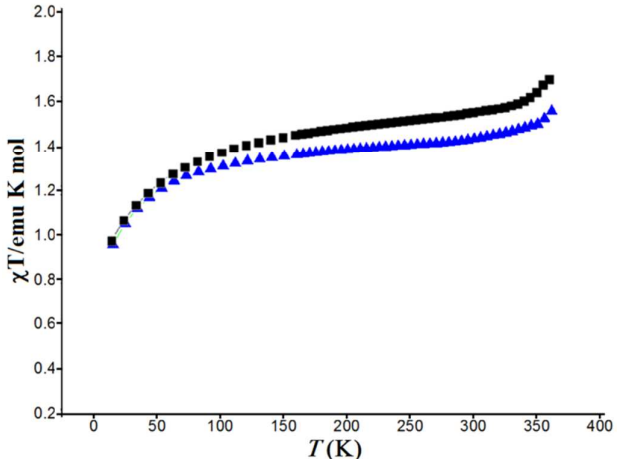

Figure S21. χT values as a function of temperature for **CPP$_2$** before (■) and after acidic treatment at pH~5 for 14h (▲)